Frequency selective phase-optimized recoupling for protons in ultra-fast solid-state magic-angle spinning NMR

Zhengfeng Zhang[1]*, Andres Oss[2], Mai-Liis Org[2], Ago Samoson[2], Huan Tan[1,3], Jun Yang[1]*

1. National Center for Magnetic Resonance in Wuhan, Key Laboratory of Magnetic Resonance in Biological Systems, State Key Laboratory of Magnetic Resonance and Atomic and Molecular Physics, Wuhan Institute of Physics and Mathematics, Innovation Academy for Precision Measurement Science and Technology, Chinese Academy of Sciences, Wuhan 430071, P.R. China.
2. Tallinn University of Technology, 19086 Tallinn, Estonia.
3. University of Chinese Academy of Sciences, Beijing 100049, P.R. China.

Correspondence: zhangzf@wipm.ac.cn (Z. Zhang), yangjun@wipm.ac.cn (J. Yang)

Abstract

We propose a new category of homonuclear frequency-selective recoupling methods for protons under ultra-fast MAS ranging from 40 kHz to 150 kHz. The methods, named as Selective Phase-optimized Recoupling (SPR) are simple in the form with defined phase schemes and RF amplitudes. SPR are robust to RF variations and efficient in frequency-selective recoupling. We demonstrated that SPR can provide a sensitivity gain of ~ 3 over the widely-used RFDR for selective $^{1}H_{N}$-$^{1}H_{N}$ correlations under 150 kHz MAS using a protonated tripeptide N-formyl-Met-Leu-Phe (fMLF). Moreover, SPR requires small ratios (~ 0.5) of RF power with respect to MAS frequency, making it perfect to probe long-range ^{1}H-^{1}H distance under ultra-fast MAS up to 150 kHz.

Solid-state nuclear magnetic resonance (NMR) spectroscopy has been applied for structural determination of insoluble proteins for over twenty years. However, the progress in this field is lagging behind other structural tools. The main reason is the difficulty to observe sufficient long-range distance restraints. Most structures of solid proteins solved by solid-state NMR are based on ^{13}C detection, which uses ^{13}C—^{13}C or ^{13}C—^{15}N distances as structural restraints. These long-range distances are difficult to be observed, due to very weak dipolar interactions that are truncated by strong dipolar interactions from shorter distances.

As the magic-angle spinning (MAS) frequencies enter the fast and ultra-fast regime, proton detection attracts more and more interest in solid-state NMR [1-9], which prefers probes with special design of MAS spinning and radio frequency (RF) [10]. Proton detection provides not only higher sensitivity per unit mass of sample but also more and longer distance restraints, because of the high gyromagnetic ratio of ^{1}H nucleus. Proton detection evolves from highly ^{1}H-diluted samples under fast MAS frequencies to fully protonated samples under ultra-fast MAS frequencies[11-21]. Current MAS frequency can go up to 140-170 kHz and the requirement on the amount of samples is reduced to the order of 0.1 mg [10,22]. The proton detection, ultra-fast MAS, and small amount of samples have shed lights on structural studies of those “tough” proteins or nucleic acids, which are too difficult or costly to prepare in large amounts.

In fully protonated molecules, the dense proton network signifies severe dipolar truncation effect. The signals from insignificant short-range ^{1}H—^{1}H distances would occupy the spectra, and cover up the weak signals from valuable long-range ^{1}H—^{1}H distances. For example, $^{1}H_N$—$^{1}H_N$ is usually truncated by stronger coupled $^{1}H_N$—$^{1}H_C$, especially for β strands (Fig. S1). With recoupling $^{1}H_N$—$^{1}H_N$ dipolar coupling while not affecting $^{1}H_N$—$^{1}H_C$ dipolar coupling would be much easier to observe the valuable $^{1}H_N$—$^{1}H_N$ distances. Partial deuteration is a way to alleviate dipolar truncation, even though much of the principally available structural information is lost. The deuteration can also cause poor yields of proteins, and is probably impractical for natural chemicals. Frequency selective recoupling is another choice to observe the correlations of interest by avoiding dipolar truncation. SEASHORE (Shift-Evolution-Assisted Selective HOmonuclear REcoupling) [23] and COMICS (COsine Modulated recoupling with Isotropic Chemical Shift reintroduction) [24] work well under slow MAS. SERP (SElective Recoupling of Protons) can provide quantitate long-range

^{1}H—^{1}H distances in fully protonated samples under ~ 70 kHz MAS, requiring the ratio of RF amplitudes (ν_1) with respect to MAS frequencies (ν_R) of ~ 1.5 [25]. BASS-SD (BAnd-Selective Spectral Spin Diffusion) performs better to selectively observe $^{1}H_N$—$^{1}H_N$ contacts than RFDR under faster MAS (e.g. 111 kHz), using low-power continuous-wave with a tailored shape [26]. In general, as the MAS frequency goes faster, new recoupling sequences prefers lower ν_1/ν_R ratios to satisfy the power handling of probes and less switching of phases (e.g. continuous-wave) to reduce deleterious effects of phase transients.

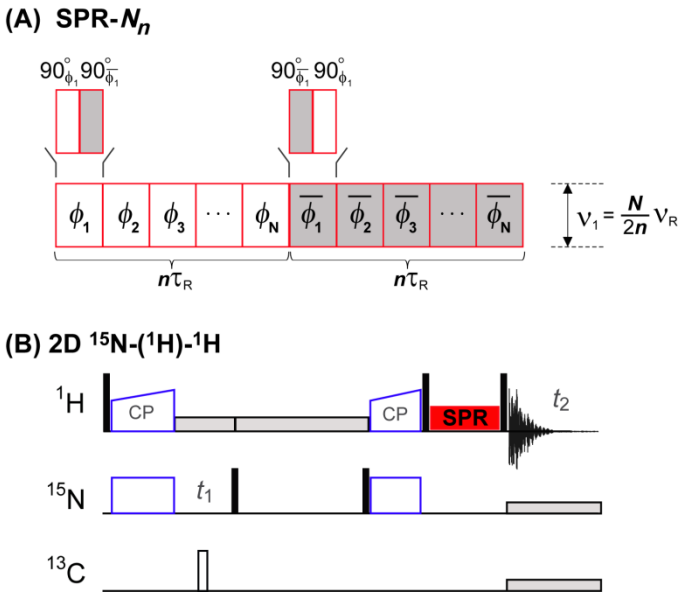

Figure 1 Pulse sequences for SPR-N_n (A) and its application in 2D ^{15}N-(^{1}H)-^{1}H experiment (B). SPR-N_n is comprised of a block with N pairs of "90 °$_x$90 °$_{-x}$" and the block repeated with a 180 °phase shift (as indicated by the bars on top of ϕ_k). The phases ϕ_k (k=1, 2, 3, …, N) are given in the supporting information. For SPR-5$_4$ and SPR-5$_6$, the phases (ϕ_1, ϕ_2, ϕ_3, ϕ_4, ϕ_5) are (0 °, 144 °, 288 °, 72 °, 216 °). SPR is incorporated into the 2D ^{15}N-(^{1}H)-^{1}H experiment used as ^{1}H-^{1}H mixing (B). MISSISSIPPI is used to suppress the residual ^{1}H signals before the second CP.[27] Heteronuclear ^{13}C/^{15}N decoupling is unnecessary during SPR.

In this study, we propose a new category of homonuclear frequency-selective recoupling methods for protons under ultra-fast MAS ranging from 40 kHz to 150 kHz. The methods, named as Selective Phase-optimized Recoupling (SPR) are simple in the form with defined phase schemes and RF amplitudes and easy to use. They are robust to RF variations and efficient in frequency-selective recoupling. We demonstrated that SPR can provide a sensitivity gain of ~ 3 over the widely-used

RFDR for selective $^{1}H_N$-$^{1}H_N$ correlations under 150 kHz MAS using a protonated tripeptide N-formyl-Met-Leu-Phe (fMLF).

SPR are as simple as *CN* symmetry-based sequences in the form [28]. SPR-N_n are comprised of a block with N pairs of "90°$_x$90°$_{-x}$" occuping n rotor periods (τ_R) and the block repeated with a 180° phase shift (Fig. 1A). The phases of SPR-N_n include all multiples of 360°/N and are simply optimized by a numerical search. While the "90°$_x$90°$_{-x}$" lays the foundation of frequency selectivity, the optimized phases make the sequences as efficient and robust as PR5 [29]. In simulations, SPR-N_n are effective with n = N-1 or N+1, where $N \geq 5$, leading to the RF amplitude $\nu_1 \approx 0.5\nu_R$. Tab. S1 shows the SPR-N_n schemes that deliver good performance in simulation. Finally, each SPR-N_n has a constant RF amplitude (ν_1) equal to $\frac{N}{2n}\nu_R$ and defined phases ϕ_k (k=1, 2, 3, …, N). That means SPR-N_n are also simple in operation, with no need to optimize the shapes, RF amplitude, modulated frequency, etc. SPR-5_4 (ν_1 = $0.625\nu_R$) and SPR-5_6 (ν_1 = $0.417\nu_R$) are the simplest in phases, sharing the same phase scheme (ϕ_1, ϕ_2, ϕ_3, ϕ_4, ϕ_5) = (0°, 144°, 288°, 72°, 216°) (Tab. S1). For simplicity, SPR-5_4 and SPR-5_6 are taken as examples in the following sections. Other SPR-N_n with n = N-1 are similar to SPR-5_4, and others with n = N+1 be similar to SPR-5_6.

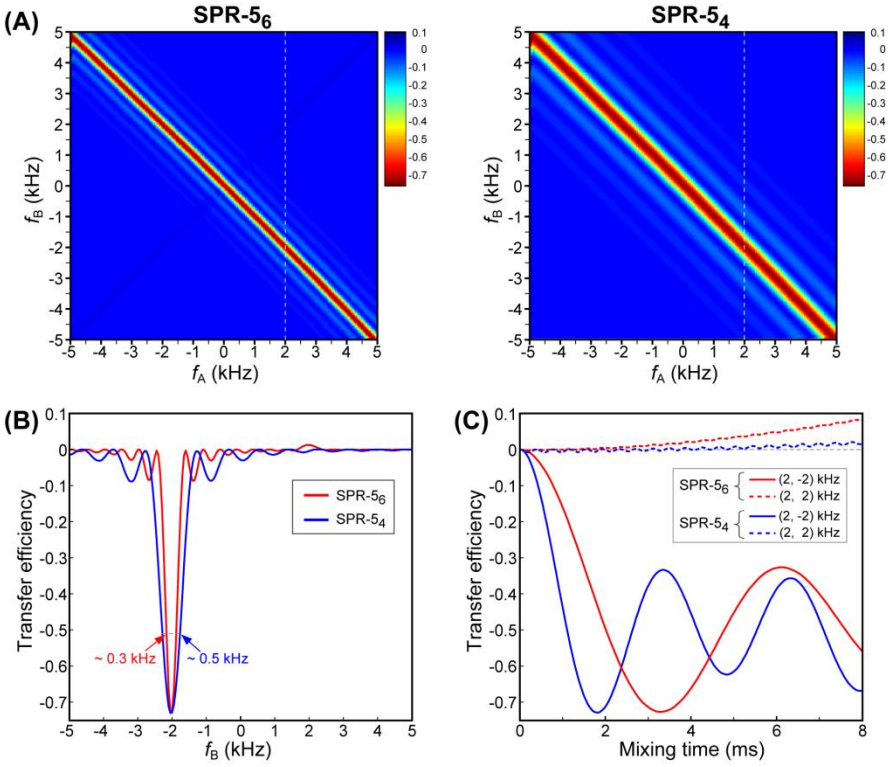

Figure 2 Simulated polarization transfer of $I_A^Z \rightarrow I_B^Z$ as functions of frequency offsets

(A and B) and mixing times (C) of SPR under 150 kHz MAS frequency. Two spins (^1H_A, ^1H_B) with a dipolar coupling of 2000 Hz (corresponding to a ^1H_A—^1H_B distance of ~ 3.92 Å) are used for simulations. The f_A and f_B represent the frequency offsets of ^1H_A and ^1H_B, respectively. In (B), the curves are extracted from (A) along the dashed lines with f_A = 2 kHz. The arrows indicate the bandwidths. In (C), the build-up curves are shown for (f_A, f_B) = (2, -2) kHz (solid lines) or (2, 2) kHz (dashed lines). SPR-5_6 and SPR-5_4 are indicated in red and in blue, respectively. Simulations were performed using the Simpson software.[30]

SPR can selectively recouple the dipolar coupling of two spins with symmetric frequency offsets (i.e. $f_A = -f_B$, where f_A and f_B represent the frequency offsets for ^1H_A and ^1H_B, respectively), as indicated by the profiles of polarization transfer versus frequency offsets (Fig. 2A and B). The negative polarization transfer efficiency indicates a DQ recoupling mechanism. Similar to SERP [31], SPR also realizes zero-quantum (ZQ) recoupling when $f_A = f_B$ (Fig. 2C). The simulated efficiency of ZQ recoupling decreases from ~ 0.4 to less than 0.1 as the MAS frequency increasing from 40 kHz to 150 kHz. Under 150 kHz MAS spinning, ZQ recoupling becomes negligible and DQ recoupling prevails in both transfer efficiencies and transfer rates and (Figs. S2). According to the DQ condition (i.e. $f_A = -f_B$), SPR can facilitate selective recoupling of ^1H_N-^1H_N by placing the transmitter frequency at the center of the ^1H_N region, and enhance selective recoupling of ^1H_N-^1H_C by placing the transmitter at the center of the ^1H_N ~ ^1H_C region. The polarization transfer reaches the maximal efficiency at the position of $f_A \approx -f_B$, and fades oscillatorily. The bandwidth (defined as the width at 70% of maxima) of SPR-5_4 ($\nu_1 = 0.625\nu_R$) is ~ 0.5 kHz and that of SPR-5_6 ($\nu_1 = 0.417\nu_R$) is ~ 0.3 kHz (Fig. 2B). The difference in bandwidth results from the combinations of (N, n) rather than the different RF amplitudes in the two schemes. Simulations show that the bandwidths of SPR-5_6 and SPR-5_4 are slightly affected by MAS frequencies and associated RF amplitudes (Fig. S3).

SPR has larger scaling factor than previous SERP [31]. While the scaling factor of SPR-5_4 is larger than that of SERP with a total phase of 480 °, the scaling factor of SPR-5_6 is larger than that of SERP with a total phase of 680 °, according to the buildup curves (Fig. 2C). The large scaling factor, which means rapid polarization transfer and hence short recoupling time for optimal transfer efficiency, is crucial to probe

long-range distances. SPR-5_4 has larger scaling factor than SPR-5_6, leading to optimal mixing times of ~ 1.8 ms and ~ 3.2 ms for SPR-5_4 and SPR-5_6, respectively, with a dipolar coupling of 2 kHz (corresponding to a ^{1}H-^{1}H distance of ~ 3.92 Å). Surprisingly, the maximal DQ transfer efficiency of SPR is ~ 0.73, numerically equal to that of γ-encoded recoupling sequences. Similar efficiency has been also achieved in the non-γ-encoded PR5 [29], suggesting that the efficiency up to 0.73 is probably not an exclusive feature of γ-encoded sequences [32]. Owing to the frequency selectivity, large scaling factor and high efficiency of the recoupling, SPR is promising for distance measurements via the DQ recoupling mechanism.

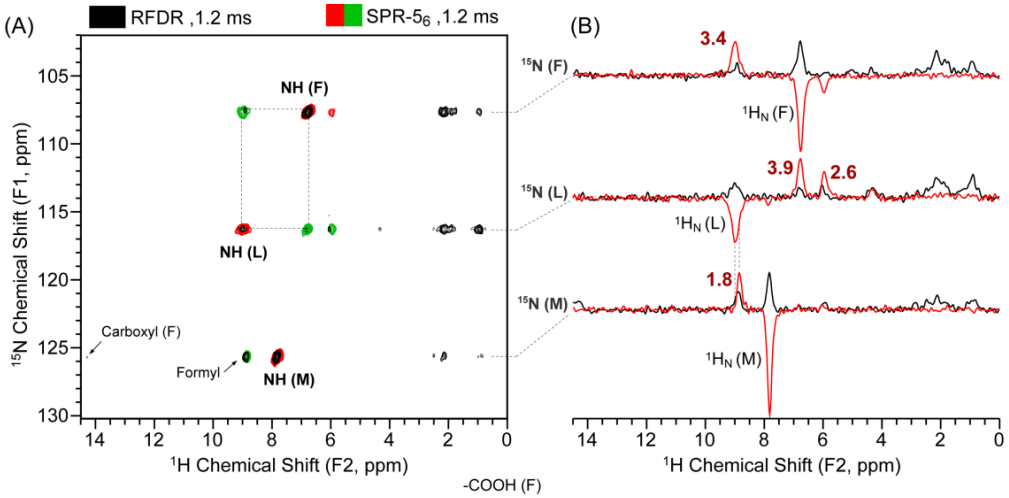

Figure 3 2D N(H)H spectra (A) and slices (B) of U-^{13}C, ^{15}N labeled N-formyl-Met-Leu-Phe (fMLF) using RFDR (black, 1.2 ms) and SPR-5_6 (red/green, 1.2 ms) under 150 kHz MAS. The ^{1}H transmitter frequency is set at 6.1 ppm. The figures represent the sensitivity gains of SPR-5_6 over RFDR. The ^{1}H RF amplitudes were ~ 62.5 kHz ($0.417\nu_R$) for SPR-5_6 and 312.5 kHz for RFDR, respectively. The data were processed with the same parameters (except for phases) and plotted with the same contour levels in Topspin.

We demonstrated the performance of SPR under ultra-fast MAS using a tripeptide N-formyl-Met-Leu-Phe (fMLF). Preliminary experiments under 100 kHz MAS show that the target peaks as well as the source peaks are more intensive in SPR-5_6 than in SPR-5_4 (Fig. S4). Overall, SPR-5_6 is superior to SPR-5_4 in both frequency selectivity and transfer efficiency. For this reason, we will focus on the comparison of SPR-5_6 and the widely-used RFDR [33,34]. Unlike the broadbanded RFDR, SPR-5_6 selects the polarization transfer only among nuclei with specific frequency offsets. The

selectivity makes SPR-5_6 also more efficient than RFDR. The averaged sensitivity gain of SPR-5_6 over RFDR is ~ 3 for polarization transfer from ^1H_N to other ^1H_N or ^1H with chemical shifts around the ^1H_N region (Fig. 3). The slice along ^{15}N (F) at 107.6 ppm gives a sensitivity gain of 3.4 for ^1H_N (F) → ^1H_N (L). The sign of ^1H_N (L) is opposite to that of ^1H_N (F), verifying the DQ transfer mechanism. The peak of $^1H_{CA}$ (M) at 6.0 ppm has the same sign as ^1H_N (F), resulting from two steps of DQ transfer, i.e. ^1H_N (F) → ^1H_N (L) and ^1H_N (L) → $^1H_{CA}$ (M). The one-step ZQ transfer of ^1H_N (F) → $^1H_{CA}$ (M) could be excluded, which would also generate the same sign as the source nuclei, because the mixing time (1.2 ms) is too short to give considerable ZQ transfer efficiency according to the build-up curve (Fig. 2C). The slice along ^{15}N (L) at 116.2 ppm gives a sensitivity gain of 3.9 for ^1H_N (L) → ^1H_N (F) and 2.6 for ^1H_N (L) → $^1H_{CA}$ (M). The higher gain of ^1H_N (L) → ^1H_N (F) can be attributed to favorable frequency offsets, even though the distance of ^1H_N (L) —^1H_N (F) (2.69 Å) is longer than that of ^1H_N (L) —$^1H_{CA}$ (M) (2.35 Å). There is a peak at 8.9 ppm in the slice along ^{15}N (M) at 125.6 ppm. This peak belongs to the formyl ^1H instead of ^1H_N (L) at 9.0 ppm, because the distance between ^1H_N (M) and the formyl ^1H (2.30 Å) is much shorter than that of ^1H_N (M) —^1H_N (L) (4.39 Å), and because no obvious transfer from ^1H_N (L) to ^1H_N (M) could be seen in the slice along ^{15}N (L) at 116.2 ppm. Resulting from the unfavorable frequency offset, the gain of 1.8 for ^1H_N (M) → ^1H (formyl) is a bit lower than others. With proper frequency offsets, the gain for transfer from ^1H_N (M) to other nuclei can also be greater than 3 (Fig. S5)

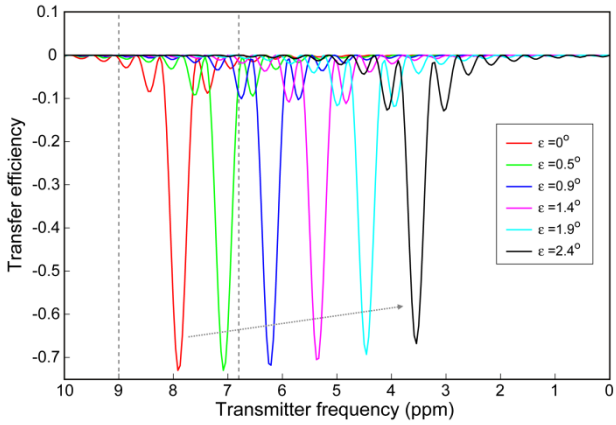

Figure 4 Effects of asymmetrical phase transient on the simulated polarization transfer of $I_A^z \rightarrow I_B^z$ of SPR-5_6 under 150 kHz MAS. In simulations, normal 90 $°_x$ is replaced by $\varepsilon_y 90\,°_x \varepsilon_{-y}$, where ε represents the flip angle of asymmetric RF phase transient. Simulations were performed on a system with two proton spins (^1H_A, ^1H_B) under 600 MHz ^1H Larmor frequency. The two dashed lines indicate the chemical

shifts of (^1H_A, ^1H_B). The dashed arrow indicates the shift of optimal transmitter frequency due to ε.

Optimal polarization transfer should occur at the position of $f_A \approx -f_B$ according to the simulations (Fig. 2), i.e., the transmitter frequency should be set in the middle of two resonance lines. However, while the SPR-5_6 experiments under 40 kHz MAS follow the simulations well (Figs. S6 and S7), the experiments under 150 kHz MAS did not reach optimal polarization at the position of $f_A \approx -f_B$ (Figs. 3 and S5). There is a deviation of ~ 1 kHz from the simulated condition. The disagreement between experiments and simulations under the ultra-fast MAS (150 kHz) is caused by asymmetric phase transient of RF pulses. The asymmetrical phase transient of a 90°_x pulse can be represented by $\varepsilon_y 90^\circ_x \varepsilon_{-y}$, where ε is the flip angle of asymmetric RF phase transient. Figure 4 shows the effects of ε on the optimal transmitter frequency for polarization transfer from ^1H_A (6.8 ppm) to ^1H_B (9.0 ppm). The optimal transmitter frequency is supposed to be at 7.9 ppm without asymmetrical phase transient (i.e. ε = 0). As the ε increases from 0 to 2.4 °, the optimal transmitter frequency is shifted from 7.9 ppm to ~ 3.5 ppm. Meanwhile, the asymmetrical phase transient would reduce the optimal transfer efficiency somewhat. Based on the experimental and simulated results (Figs. 3 and 4), the asymmetrical phase transient must exist with ε equal ~ 1 ° under the experimental condition, which shifts the optimal transmitter frequency from 7.9 ppm to ~ 6.1 ppm. With the ε of ~ 1 °, the efficiency of SPR is barely affected even under 150 kHz MAS. The result highlights the importance of RF phase transient under ultra-fast MAS. It is important to develop recoupling sequences with lower RF power like SPR, which would lead to longer RF pulses and less demanding on phase switching, to reduce the deleterious effects of phase transient.

In conclusion, we have developed SPR to selectively recouple ^1H-^1H correlations in fully protonated samples under ultra-fast MAS conditions. SPR is simple, robust and efficient in frequency selective recoupling, which serves as a potential technique to obtain useful restraints for structural determination. It can also be used in a constant-time way to quantitative measurements of distances[31,35]. Compared to the widely-used RFDR, SPR provides sensitivity gains up to 3 for selective ^1H–^1H correlations (e.g. ^1H_N–^1H_N). Moreover, SPR requires small ratios of RF power with respect to MAS frequency, making it perfect to probe long-range ^1H-^1H distance

under ultra-fast MAS up to 150 kHz.

Acknowledgements

This work was supported by grants from the National Natural Science Foundation of China (21775161, 31627803, 31770798 and 21927801) and the National Key R&D Program of China (2016YFA0501200, 2017YFA0505400) (to Z. Z. and J. Y.) and supported by Estonian Research Agency (to A. O., M. O. and A. S.). We are very grateful to Dr. Robert Tycko (National Institutes of Health) for helpful discussions. We thank Dr. Liying Wang and Mr. Zhi Ren for help with the NMR facilities.

References

(1) Ishii, Y.; Tycko, R. *J. Magn. Reson.* **2000**, *142*, 199.

(2) Ishii, Y.; Yesinowski, J. P.; Tycko, R. *J. Am. Chem. Soc.* **2001**, *123*, 2921.

(3) Hologne, M.; Faelber, K.; Diehl, A.; Reif, B. *J. Am. Chem. Soc.* **2005**, *127*, 11208.

(4) Chevelkov, V.; Rehbein, K.; Diehl, A.; Reif, B. *Angew. Chem. Int. Ed.* **2006**, *45*, 3878.

(5) Zhou, D. H.; Shah, G.; Cormos, M.; Mullen, C.; Sandoz, D.; Rienstra, C. M. *J. Am. Chem. Soc.* **2007**, *129*, 11791.

(6) Zhou, D. H.; Shea, J. J.; Nieuwkoop, A. J.; Franks, W. T.; Wylie, B. J.; Mullen, C.; Sandoz, D.; Rienstra, C. M. *Angew. Chem. Int. Ed.* **2007**, *46*, 8380.

(7) Zhou, D. H.; Shah, G.; Mullen, C.; Sandoz, D.; Rienstra, C. M. *Angew. Chem. Int. Ed.* **2009**, *48*, 1253.

(8) Schubeis, T.; Le Marchand, T.; Andreas, L. B.; Pintacuda, G. *J. Magn. Reson.* **2018**, *287*, 140.

(9) Penzel, S.; Oss, A.; Org, M. L.; Samoson, A.; Bockmann, A.; Ernst, M.; Meier, B. H. *J. Biomol. NMR* **2019**, *73*, 19.

(10) Samoson, A. *J. Magn. Reson.* **2019**, *306*, 167.

(11) Asami, S.; Schmieder, P.; Reif, B. *J. Am. Chem. Soc.* **2010**, *132*, 15133.

(12) Linser, R.; Bardiaux, B.; Higman, V.; Fink, U.; Reif, B. *J. Am. Chem. Soc.* **2011**, *133*, 5905.

(13) Reif, B. *J. Magn. Reson.* **2012**, *216*, 1.

(14) Asami, S.; Reif, B. *Acc. Chem. Res.* **2013**, *46*, 2089.

(15) Nieuwkoop, A. J.; Franks, W. T.; Rehbein, K.; Diehl, A.; Akbey, U.; Engelke, F.; Emsley, L.; Pintacuda, G.; Oschkinat, H. *J. Biomol. NMR* **2015**, *61*, 161.

(16) Medeiros-Silva, J.; Mance, D.; Daniels, M.; Jekhmane, S.; Houben, K.; Baldus, M.; Weingarth, M. *Angew. Chem. Int. Ed.* **2016**, *55*, 13606.

(17) Vasa, S. K.; Rovo, P.; Giller, K.; Becker, S.; Linser, R. *PCCP* **2016**, *18*, 8359.

(18) Andreas, L. B.; Jaudzems, K.; Stanek, J.; Lalli, D.; Bertarello, A.; Le Marchand, T.; Paepe, D. C. D.; Kotelovica, S.; Akopjana, I.; Knott, B.; Wegner, S.; Engelke, F.; Lesage, A.; Emsley, L.; Tars, K.; Herrmann, T.; Pintacuda, G. *Proc. Natl. Acad. Sci. U.S.A.* **2016**, *113*, 9187.

(19) Lalli, D.; Idso, M. N.; Andreas, L. B.; Hussain, S.; Baxter, N.; Han, S.; Chmelka, B. F.; Pintacuda, G. *J. Am. Chem. Soc.* **2017**, *139*, 13006.

(20) Marchanka, A.; Stanek, J.; Pintacuda, G.; Carlomagno, T. *Chem. Commun*. **2018**, *54*, 8972.

(21) Xiang, S. Q.; le Paige, U. B.; Horn, V.; Houben, K.; Baldus, M.; van Ingen, H. *Angew. Chem. Int. Ed.* **2018**, *57*, 4571.

(22) Lin, Y. L.; Cheng, Y. S.; Ho, C. I.; Guo, Z. H.; Huang, S. J.; Org, M. L.; Oss, A.; Samoson, A.; Chan, J. C. C. *Chem. Commun.* **2018**, *54*, 10459.

(23) Paravastu, A. K.; Tycko, R. *J. Chem. Phys.* **2006**, *124*, 194303.

(24) De Paepe, G.; Lewandowski, J. R.; Griffin, R. G. *J. Chem. Phys.* **2008**, *128*.

(25) Vinogradov, E.; Madhu, P. K.; Vega, S. *Chem. Phys. Lett.* **1999**, *314*, 443.

(26) Jain, M. G.; Lalli, D.; Stanek, J.; Gowda, C.; Prakash, S.; Schwarzer, T. S.; Schubeis, T.; Castiglione, K.; Andreas, L. B.; Madhu, P. K.; Pintacuda, G.; Agarwal, V. *J. Phys. Chem. Lett.* **2017**, *8*, 2399.

(27) Zhou, D. H.; Rienstra, C. M. *J. Magn. Reson.* **2008**, *192*, 167.

(28) Levitt, M. H. In *Encyclopedia of Nuclear Magnetic Resonance*; Grant, D. M., Harris, R. K., Eds.; Wiley: Chichester, 2002; Vol. 9, p 165.

(29) Zhang, Z. F.; Liu, H.; Deng, J.; Tycko, R.; Yang, J. *J. Chem. Phys.* **2019**, *150*, 154201.

(30) Bak, M.; Rasmussen, J. T.; Nielsen, N. C. *J. Magn. Reson.* **2000**, *147*, 296.

(31) Duong, N. T.; Raran-Kurussi, S.; Nishiyama, Y.; Agarwal, V. *J. Phys. Chem. Lett.* **2018**, *9*, 5948.

(32) Nielsen, N. C.; Bildsoe, H.; Jakobsen, H. J.; Levitt, M. H. *J. Chem. Phys.* **1994**, *101*, 1805.

(33) Bennett, A. E.; Ok, J. H.; Griffin, R. G.; Vega, S. *J. Chem. Phys.* **1992**, *96*, 8624.

(34) Ishii, Y. *J. Chem. Phys.* **2001**, *114*, 8473.

(35) Tycko, R. *J. Chem. Phys.* **2007**, *126*, 064506.